

Revue des Composites et des Matériaux Avancés-Journal of Composite and Advanced Materials

Vol. 35, No. 5, October, 2025, pp. 947-955

Journal homepage: http://iieta.org/journals/rcma

Synthesis and Characterization of Tungsten Carbide (WC)-Based Nanocomposites and Their Optical Properties and Corrosion Behavior



Salahaldin Mansur Alduwaib* Muhannad Mahdi Abd

Department of Science, College of Basic Education, Mustansiriyah University, Baghdad 10001, Iraq

Corresponding Author Email: salah.aldin@uomustansiriyah.edu.iq

Copyright: ©2025 The authors. This article is published by IIETA and is licensed under the CC BY 4.0 license (http://creativecommons.org/licenses/by/4.0/).

https://doi.org/10.18280/rcma.350514

Received: 16 August 2025 Revised: 24 September 2025 Accepted: 19 October 2025 Available online: 31 October 2025

Keywords:

tungsten carbide, graphene, carbon nanotubes, corrosion, optical properties

ABSTRACT

Many materials are known for their remarkable uses in modern research, including tungsten carbide (WC), which has many hardness characteristics, such as high toughness and notable chemical resistance. Because of its stability, it is essential in a variety of industrial sectors, particularly in cutting tools and coatings used in applications that are resistant to wear. WC nanoparticles were created using the hydrothermal synthesis technique. A composite that improves structural stability and functional efficacy is created when WC nanoparticles are added to graphene (G) and carbon nanotubes (CNTs). Verifying the materials' structural, physical, and chemical characteristics is the aim of the characterizations carried out for this investigation. WC and its composites were validated using a range of methods, such as energy-dispersive X-ray spectroscopy (EDXS), fieldemission scanning electron microscopy (FESEM), and X-ray diffraction (XRD) analyses. The electronic and optical properties of the materials were also revealed by Raman, UV-Visible, and photoluminescence (PL) spectroscopy, which demonstrated that the band gap characteristics are considerably changed by the addition of carbon nanostructures. When WC nanoparticles encapsulated with graphene (WC-G) and carbon nanotubes (WC-CNT), it exhibited noticeably superior corrosion resistance compared to pure tungsten carbide, these results are revealed by electrochemical tests.

1. INTRODUCTION

The intrinsic qualities of tungsten carbide (WC), including durability, tensile strength, and resistance to chemical interactions, are widely recognized as essential characteristics in demanding industrial settings as protective coatings, wearresistant components, and structural reinforcements, especially in industries where corrosion and mechanical stress are common [1]. However, as engineering uses become more complicated, traditional WC materials have come close to reaching the limits of what they can do. This has made more people interested in nanostructured alternatives. Nanotechnology has been added to materials science, which has made it possible to make tungsten carbide in nanoparticulate form. This opens up new ways to improve its excellent mechanical and chemical properties. WC has better wear resistance, toughness, and surface stability at the nanoscale. The enhanced specific surface area and the complex grain architecture are primarily responsible for these improvements [2, 3]. These developments not only help WCbased systems last longer and perform better, but they also make it easier to design components that are more specifically suited, increasing the systems' effectiveness for complex industrial applications [4, 5].

Corrosion is still a big problem in many areas, such as aerospace, marine engineering, and cars. When materials

break down like this, it costs more to keep them in good shape and makes work less efficient. People know that tungsten carbide (WC) is very strong and doesn't wear out easily, but it doesn't work well in corrosive conditions because it breaks down and oxidizes easily [6, 7]. Recent research has alleviated these limitations by incorporating carbon-based nanoparticles into WC matrices. Graphene (G) [8, 9] and carbon nanotubes (CNTs) [10, 11] have been used to make composites that work better overall. These carbon-based reinforcements have a lot of benefits that work together. The most important thing they do is make the composites stronger and better at conducting electricity. More importantly, they help make thick protective layers that stop processes that break things down. This makes coatings made with WC last longer [12, 13]. Graphene and CNTs also have a lot of surface area and are naturally stable, which makes them even better at stopping pathways that lead to electrochemical breakdown [14, 15].

Various studies have been conducted on WC-based composites, including carbon-based nanomaterials. In the study done by Guan et al. [16], the effects of WC on thermal and mechanical attributes of carbon fiber (CF)/copper (Cu) binary composites were investigated. The results revealed that the incorporation of WC into the binary CF/Cu system improves its thermal and mechanical properties, which originates from the effective role of WC in enhancing the interface bonding between Cu and CF and subsequently,

diminishing the poor interface bonding between the two components [16]. In another study, the fabricated composite exhibited higher tensile strength compared to pure Cu and also the binary system of CNTs/Cu, which was attributed to role of WC in creating robust interfacial bonding among components. The robust interface bonding not only enhanced tensile strength but also improved the electrical and thermal conductivity of the binary composite [17].

Researchers have devised several ways to make tungsten carbide nanoparticles, such as mechanical alloying, chemical vapor deposition (CVD), sol-gel processing, and hydrothermal synthesis. Hydrothermal synthesis is the most popular method because it is cheap, can be used on a large scale, and gives you precise control over the shape of the nanoparticles [4, 16]. This level of control makes it possible to make nanoparticles with specific sizes and shapes, which is important for improving the material's functional properties. When graphene and CNTs are added to tungsten carbide matrices, they make stronger nanocomposites less likely to corrode. These changes make the modified composites look very promising for advanced protective coatings, where long-term performance and durability are important [9, 18-20]. The carbon nanostructures and the WC matrix work together to make the material stronger than regular tungsten carbide when things get tough. We made WC nanoparticles for this study using a hydrothermal method because it is very precise and can be done again. Then, the nanoparticles were mixed with graphene and CNTs in a controlled way to make the material less likely to rust.

The research employed various characterization techniques to examine materials, like X-ray diffraction (XRD) to look at the structural properties and field emission scanning electron microscopy (FESEM) to show the morphological aspects, also chemical makeup was examined using energy-dispersive X-ray spectroscopy (EDXS). Photoluminescence (PL), Raman, and UV-Visible spectroscopy were employed to study the materials' electrical characteristics. These characterization results demonstrated the successful synthesis of three distinct materials: pure WC nanoparticles, WC-graphene (WC-G), and WC-CNT nanocomposites.

These results show that these advanced materials could be very useful in situations where corrosion is likely to happen, especially as protective coatings. This study examines practical approaches to prolong the durability of tungsten carbide by developing nanocomposites, directly addressing the persistent challenge of its insufficient corrosion resistance. The results have important effects on the development of new materials. First, they show that WC needs to be changed so that it lasts longer in tough situations. Second, they made it possible to do more research on the best protective coatings. These results give us useful information that will help us use nanomaterials more in factories where it is very important to keep things from rusting.

2. EXPERIMENTAL SECTION

2.1 Synthesis of WC nanoparticles

WC nanoparticles were made using a cheap and energy-efficient hydrothermal method [16]. The first step in making the compound was to mix 5 g of ammonium meta-tungstate (AMT), which is the source of tungsten, with warm deionized water to make a precursor solution. Then, 4.6 g of maize starch was added as the carbon precursor, and the mixture was stirred

very hard to make sure it was well mixed. The solution was then put into a stainless-steel autoclave with Teflon lining. The autoclave was tightly sealed to keep the reaction conditions the same. Hydrothermal treatment occurred at 200°C for 8 hours without mechanical stirring during the reaction period. After allowing the system to naturally cool to room temperature, the resulting contents were extracted and diluted. The precursor material was obtained by spray-drying the solution using hot air at 250°C. Finally, the tungsten carbide nanoparticles were produced by calcining the precursor material in a vacuum furnace at 980°C for 1 hour.

2.2 Synthesis of graphene nanosheets

Synthesis of graphene is typically done by means of various techniques [21]. However, in this work, graphene nanopowder was prepared from the US Nano Company and used without additional purification

2.3 Synthesis of carbon nanotubes via chemical vapor deposition method

CNTs were fabricated using the CVD method. The first thing that had to be done was to produce a catalyst. To maintain the iron structure stable, magnetite (Fe₃O₄) was mixed with aluminum oxide (Al₂O₃, 2.9%) and calcium oxide (CaO, 3.0%) [22]. An electric furnace was utilized to cook the catalyst mixture, then crushed it and used a screen to get particles that were between 1.2 and 1.5 mm in size. Next, the catalyst was lowered while hydrogen flowed over it at 500°C for an hour. This turned iron nanoparticles into nanocrystalline iron. They put the iron catalyst that they had manufactured in a quartz boat and put it in an extremely hot furnace. Before the reaction started, the catalyst was heated up, and hydrogen gas was blown over it to get rid of any dirt on the surface. When the catalyst was ready, ethylene gas (C₂H₄) was put into the furnace at a rate of 5 to 10 L per hour. The reaction happened at 700°C for an hour. The ethylene broke down, and the carbon atoms gathered together to become multi-walled carbon nanotubes (MWCNTs) during that time. After the reaction, some samples underwent hydrogenation at 500°C to decompose any remaining iron carbide (Fe₃C) into iron and carbon. This step promoted the agglomeration of small iron particles into larger clusters, making it easier to separate them from the carbon matrix. The final product was a black, fluffy material composed of MWCNTs.

2.4 How to make nanocomposites with WC-G and WC-CNT $\,$

WC-G and WC-CNT nanocomposites were made by putting them together in a way that was easy and worked well. 50 mL of ethanol and 0.2 g of WC were mixed with 0.05 g of graphene or CNTs. To make sure that all the parts were mixed evenly, the mixture was stirred well on a hot plate. After that, the solution was carefully heated to about 60°C to get rid of the ethanol and leave a dry powder. After that, the powder was ground up into a uniform nanocomposite material. It was done three times for each study, and the data shown are typical.

3. RESULTS AND DISCUSSION

3.1 Characterization analyses

Figure 1 exhibits XRD patterns of pure WC and

nanocomposites of WC@graphene and WC@CNT. XRD is one of the most highly used characterization analyses, which is utilized for the identification of crystal structures of materials. Moreover, it is a beneficial means for estimating the average size of the particles.

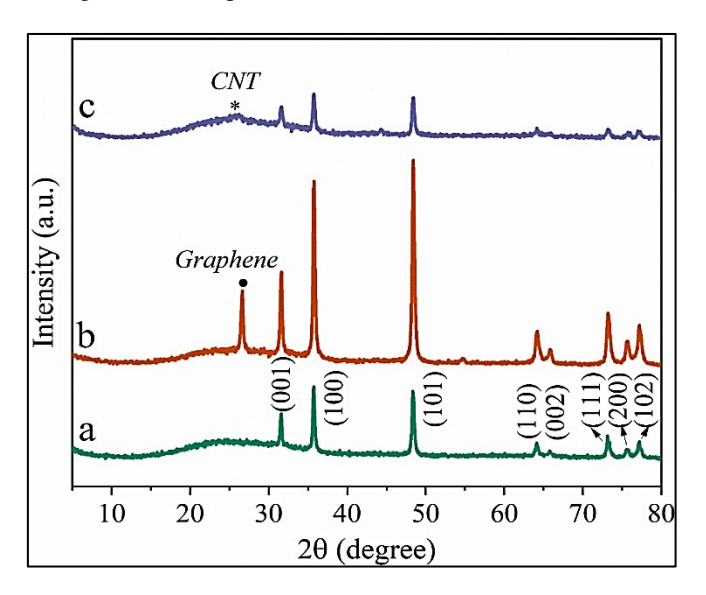


Figure 1. XRD images of (a) WC along with its nanocomposites, including (b) WC@G, and (c) WC@CNT, which are recorded from 5 to 80°

Figure 1(a) demonstrates an XRD image of pure WC, which is recorded from 5 to 80°. In this regard, different diffraction peaks are detected at 20 of 31.6, 35.7, 48.4, 64.1, 65.7, 73.1, 75.6, and 77.2°. The aforementioned peaks are respectively ascribed to crystal planes of (001), (100), (101), (110), (002), (111), (200), and (102) (JCPDS file No. 65-8828), which are assigned to hexagonal phase (P-6m2) of tungsten carbide [16, 23-25]. For the WC@G composite, in addition to diffraction peaks detected in the XRD pattern of pure WC, a new diffraction peak appears. In accordance with Figure 1(b) showing the XRD pattern of WC composited with graphene, the sharp peak located at 2θ of 26.6° is attributed to graphene's (002) crystal plane [26, 27]. In terms of the WC@CNT composite (Figure 1(c)), the diffraction peaks relevant to pure WC are obvious. Besides, another peak can be seen at 2θ of about 25.7°, which is attributed to CNTs' (002) crystal plane [28, 29]. The mean size of the particles could be estimated by means of the following relationship, known as Debye-Scherrer's formula [30]:

$$D = \frac{K\lambda}{\beta\cos\theta} \tag{1}$$

In this regard, D is assigned to mean size of the particles, K exhibits the Scherrer constant (K=0.98), λ signifies the wavelength of X-ray with the value of 1.541 Å, θ shows the Bragg angle, and β demonstrates the full width obtained at half maximum (FWHM). By using Eq. (1), the mean size of 23.5, 39.1, and 20.5 nm is respectively obtained for WC, WC@graphene, and WC@CNT.

FESEM images obtained from pure WC and its nanocomposites with either graphene or CNTs are portrayed in Figure 2. FESEM analysis is commonly hired to

morphologically scrutinize the materials. Additionally, it is capable of providing valuable information on the size of the particles. As depicted by Figure 2(a), the FESEM image of pure WC, innumerable agglomerated nanoparticles can be seen, which are evenly dispersed. The nanoparticles show no regular shape and their size changes roughly from 82 to 290 nm (Figure 2(b)).

Compositing the nanoparticles of pure WC with graphene has led to no change in their morphology. In this direction, irregular-shaped nanoparticles of pure tungsten carbide are distributed graphene sheets' surface, as demonstrated by FESEM image of WC@graphene nanocomposite (Figure 2(c)). The size of WC nanostructures in WC@graphene nanocomposite varies roughly from 66 to 240 nm (Figure 2(d)). Similar to WC@graphene, compositing tungsten carbide with CNTs caused no alteration in the morphology of WC nanostructures. Accordingly, and based on Figure 2(e), an interwoven network of carbon nanotubes is evident, on which the nanoparticles of WC are uniformly dispersed. WC nanostructures within the nanocomposite of WC@CNT demonstrate a size ranging from 58 to 152 nm (Figure 2(f)).

EDXS was another characterization test, which was designed to probe the elemental composition of the synthesized WC and its nanocomposites, including WC@graphene and WC@CNT. EDXS pattern of pure WC is illustrated in Figure 3(a).

Accordingly, the well-defined peaks of tungsten (W) element are observed at around 1.75, 7.5, 8.5, 9.75, and 11.25 keV. In addition, the peak of carbon (C) element is detectable at about 0.25 keV. The peaks of C and W elements originate from tungsten carbide nanoparticles. The weak peak of oxygen (O) element could arise from the moisture or physiosorbed carbon dioxide (CO_2) molecules.

The EDXS patterns of WC@graphene and WC@CNT nanocomposites are illustrated in Figure 3(b) and Figure 3(c), respectively. Accordingly, the noticeable peaks of W and C arising from pure WC are obviously detected. The major difference between the EDXS pattern of pure WC with that of nanocomposites is the intensity of the peak of C element. In comparison with WC, the EDXS patterns of WC@graphene and WC@CNT nanocomposites reveal a carbon peak with higher intensity, which is due to introduction of either graphene or CNTs.

Raman spectra of WC, WC@graphene, and WC@CNT are illustrated in Figure 4. In accordance with the Raman spectrum of pure WC shown in Figure 4(a), several peaks are observed. The major peaks seen at 681 and 804 cm⁻¹ pertain to the vibration of W-C bond [31, 32]. Besides, other peaks are detectable for pure WC, which are centered at 70, 235, and 4055 cm⁻¹. As evidenced by the Raman spectrum of WC composited with graphene (Figure 4(b)), the peaks showing pure WC are observed at 70, 235, 681, and 804 cm⁻¹. In addition, another peak can be found at 1578 cm⁻¹, which corresponds to G-band.

Raman spectra of the carbonaceous materials such as graphene and CNTs manifest two well-defined peaks, one of which is found at approximately 1362 cm⁻¹ (D-band), which is attributed to sp³ defects within the carbonaceous material. This peak is capable of providing information on structural imperfections as well as surface defects. D-band possesses A_{1g} symmetry and denotes the k point phonons' breathing mode [33-36].

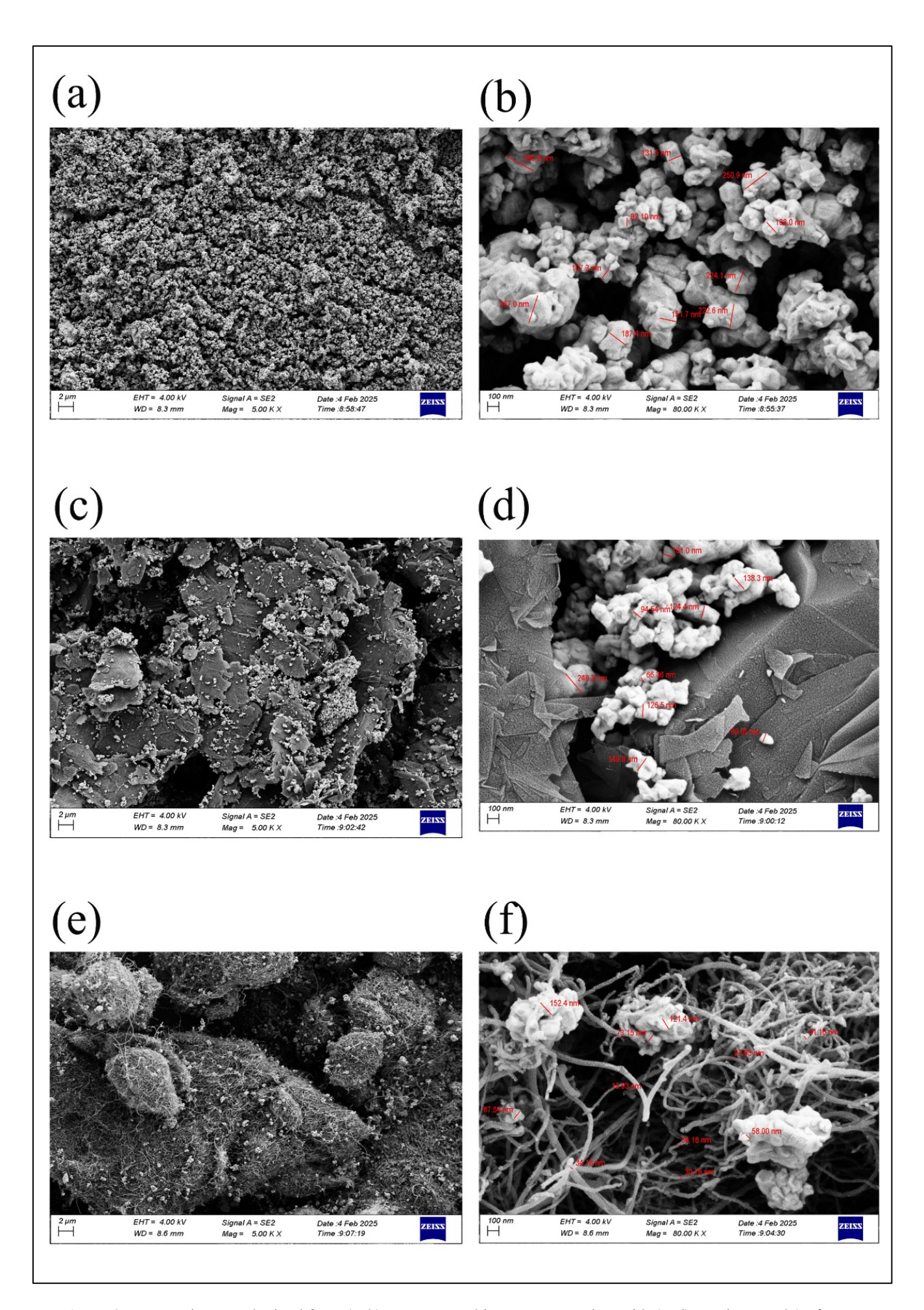


Figure 2. FESEM images obtained from (a, b) pure WC and its nanocomposites with (c, d) graphene and (e, f) CNT

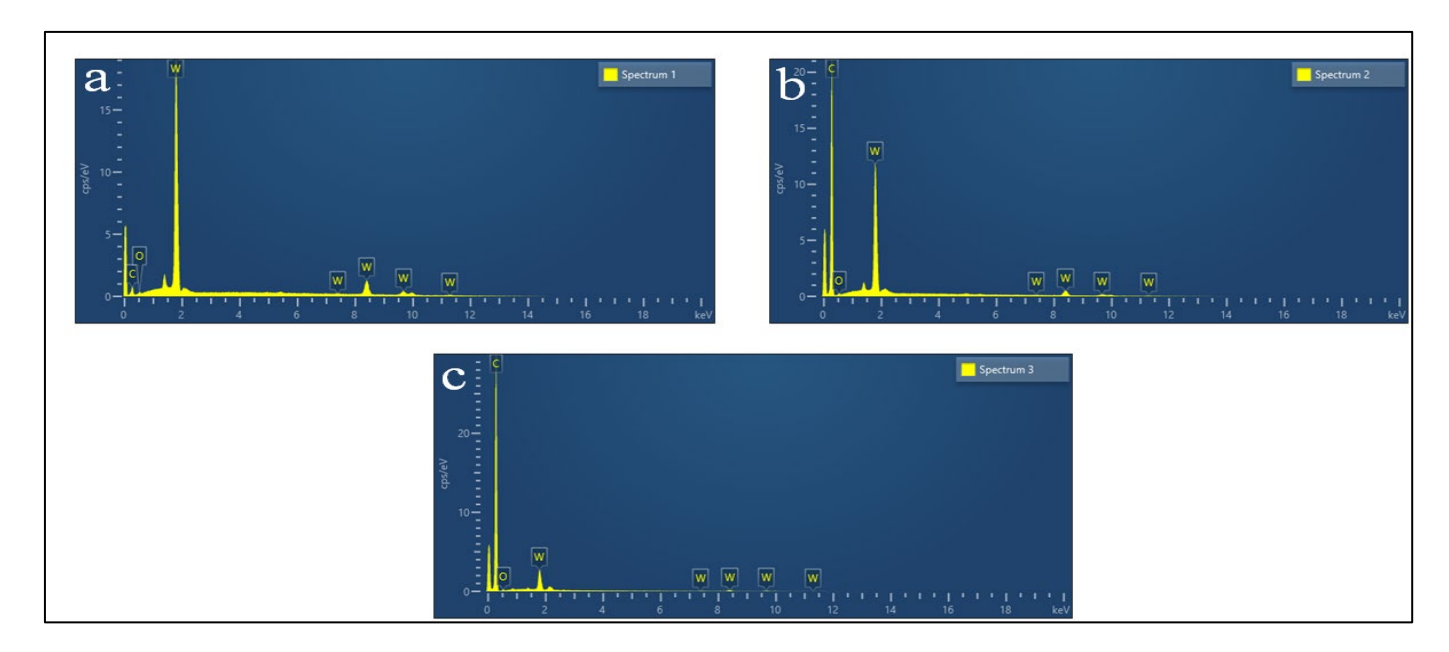


Figure 3. EDXS patterns of (a) WC and its nanocomposites with (b) graphene, and (c) CNT

The other peak is situated at about 1578 cm $^{-1}$ (G-band), which is indicative of sp 2 carbon atoms' in-plane vibration and is attributed to vibrational mode of E_{2g} . G-band features the symmetry and also crystallizability of carbon atoms [33-36]. No peak demonstrating D-band can be detected in the spectrum of WC@graphene nanocomposite. In terms of the sample composited with CNTs, the main peaks pertinent to WC nanostructures are evident (Figure 4(c)). In addition, the D- and G-bands can be found. As all the characterization tests attested, it can be come to an end that pure WC and its nanocomposites, including WC@graphene and WC@CNT, are successfully prepared.

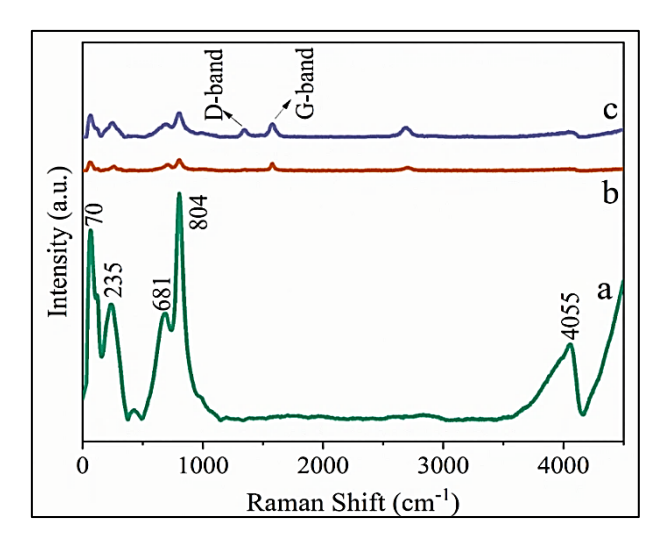


Figure 4. Raman spectra of (a) WC and its nanocomposites with (b) graphene, and (c) CNT, which are recorded in the Raman shift from 0 to 4500 cm⁻¹

3.2 Optical properties investigation

In order to examine optical properties of WC and its nanocomposites, UV-Visible spectroscopy was conducted.

According to UV-Visible spectrum of pure WC from ~200 to 1000 nm (Figure 5), an attenuated absorption peak is detectable at about 270 nm, which is located in the UV region. Compositing pure WC with graphene has given rise to no

change in its absorbance spectrum. In this regard, the weak absorption peak found for pure WC can also be seen in the UV-Visible absorbance spectrum of WC@graphene nanocomposite. Like other samples, the nanocomposite of WC@CNT demonstrates the absorption peak at 270 nm.

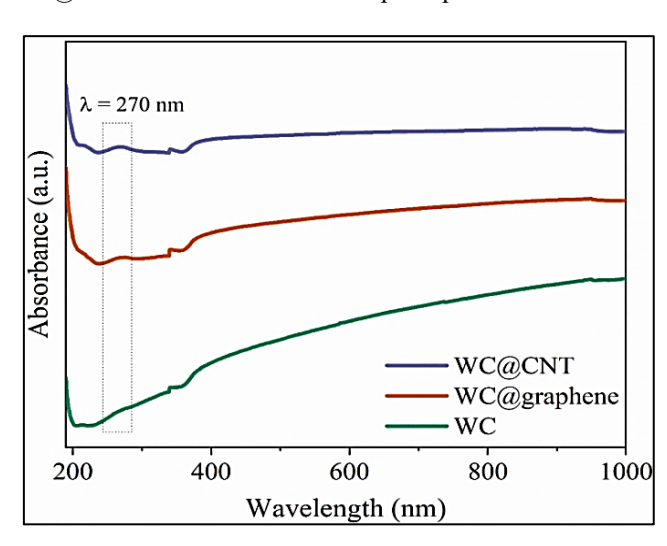


Figure 5. UV-Visible absorbance spectra of the samples from ~200 to 1000 nm

To investigate the energy band gap (E_g) factor, the Tauc's plots of the samples were plotted (Figure 6). In this regard, the straight line obtained through plotting $(\alpha hv)^2$ versus photon energy (hv) is extrapolated to horizontal axis, with the aid of which the energy band gap of the samples is calculated. In the Tauc's plot, α denotes the material's absorption coefficient, h represents Planck's constant, and v shows the frequency of the light [37, 38].

In accordance with Figure 6, the energy band gap calculated for WC, WC@graphene, and WC@CNT, respectively, is 6.28, 6.15, and 5.63 eV. As a consequence, compositing pure WC with either graphene or CNTs caused a reduction in the energy band gap. The lower energy band gap corresponds shorter distance between the valence and conduction bands, which facilitates the electron transition between the two bands and subsequently, improves photocatalytic properties.

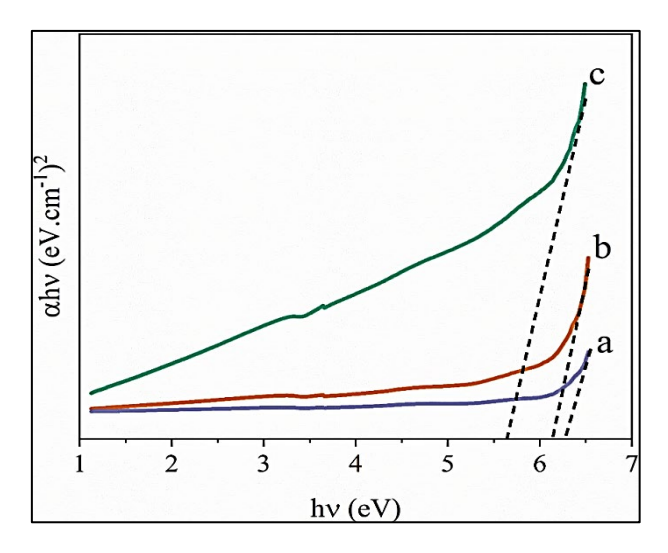


Figure 6. The energy band gap of (a) WC, (b) WC@graphene, and (c) WC@CNT

In addition to UV-Visible spectroscopy, PL spectroscopy was adopted to investigate the optical characteristics of samples. According to Figure 7 showing the PL spectra of pure WC and its nanocomposites, two sharp peaks can be detected, one of which is situated at 309 nm (UV area) and the other is found at 619 nm (visible region).

Obviously, the PL peaks of the composites are more intense than pure WC. These results are in a well agreement with energy band gap values where WC@graphene and WC@CNT nanocomposites demonstrated less Eg in comparison with pure WC. Both graphene and CNT reduced the bandgap of WC material; hence, the pathways are more efficient for the electrons.

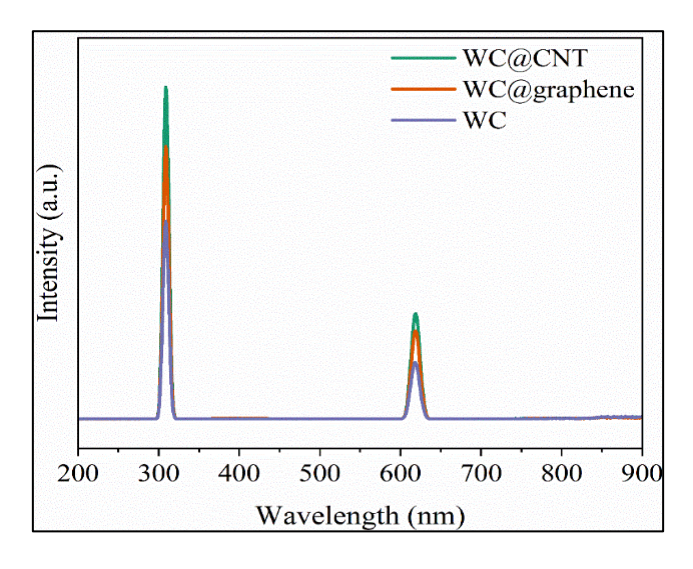


Figure 7. PL spectra of WC, WC@G, and WC@CNT

3.3 Corrosion resistance and corrosion inhibitory measurements

Figure 8 demonstrates Nyquist plots recorded for the bare stainless steel and the ones coated with WC, WC@graphene, and WC@CNT. The inset equivalent circuit was adopted for fitting the plots. In this regard, R_s, R_{ct}, and CPE are respectively ascribed to resistance of solution, charge transfer resistance, and constant phase element, which are tabulated in Table 1.

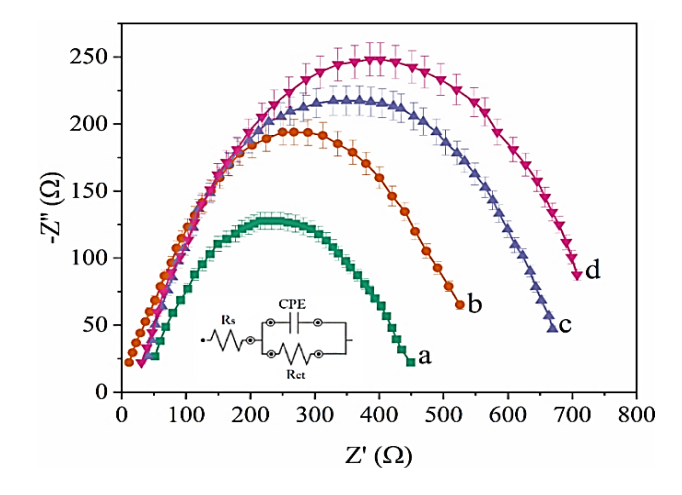


Figure 8. The Nyquist plots taken for (a) the bare stainless steel and the ones coated with (b) WC, (c) WC@G, and (d) WC@CNT (inset is the equivalent circuit)

Table 1. The results obtained from the fitting of Nyquist plots of the samples

Sample	Rs	Rct
Stainless steel	51.71	448.86
WC	11.66	525.46
WC@graphene	40.66	669.44
WC@CNT	30.69	707.26

Accordingly, the R_{ct} shown by the bare stainless steel is 448.86 Ω . Obviously, coating it with WC resulted in an increase in charge transfer resistance. In this direction, the R_{ct} delivered by the sample with WC is 525.46 Ω . Including either graphene or CNT into WC increased R_{ct} . To this end, the charge transfer resistances obtained for WC@graphene and WC@CNT, respectively, are 669.44 and 707.26 Ω .

Referring to literature, R_{ct} indicates the difficulty of transferring the charges on the surface of the coating. In other words, the higher value of R_{ct} means the higher resistance of the coating against corrosion [39]. Therefore, WC@graphene and WC@CNT nanocomposites could outperform pure WC in protecting stainless steel from corrosion.

The WC and its nanocomposites' corrosion inhibitory was examined by monitoring their open circuit potential (E_{OCP}). In equilibrium state of system, the E_{OCP} and free corrosion potential corresponded, and also on the surface of metal shown no net electric current passes. This factor is valuable for inhibitory properties of materials [40].

For E_{OCP} measurements, a three-electrode system was adopted where the bare stainless steel or its counterpart coated with our sample was assigned as the working electrode. Moreover, Ag/AgCl and Pt wire were respectively employed as the reference and counter electrodes. All the electrodes were immersed in a 3.0 wt% NaCl aqueous solution.

According to Figure 9(a), showing the OCP-time curve of the free sample (bare stainless steel), the potential reached a steady state after 1000 s. Changing the bare stainless steel working electrode to WC-coated stainless steel has resulted in a movement of potential toward more positive values (Figure 9b), signifying that this sample was less exposed to corrosion. Compositing pure WC with either graphene or CNTs shifted its open circuit potential to more positive values (Figures 9(c) and (d)), meaning that WC@graphene and WC@CNT nanocomposites are less corrosion-prone compared to other samples. As a result, WC and its nanocomposites could be

ideal candidates for corrosion inhibitory purposes (Figure 10).

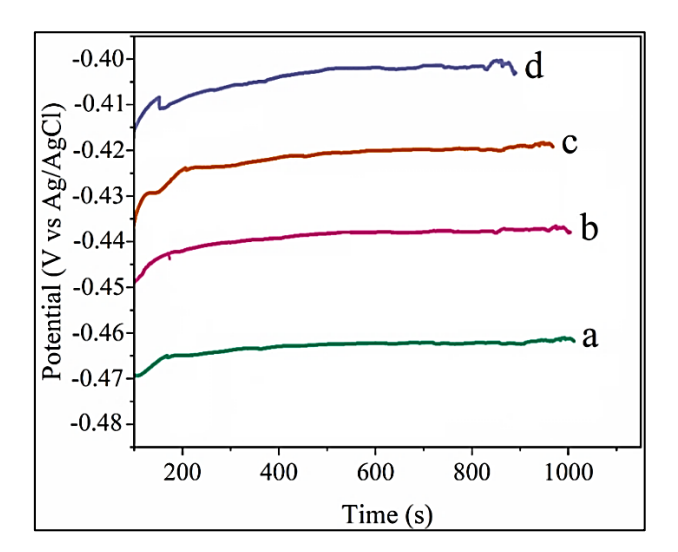


Figure 9. OCP-time plots for (a) the bare stainless steel and the ones coated with (b) WC, (c) WC@G, and (d) WC@CNT

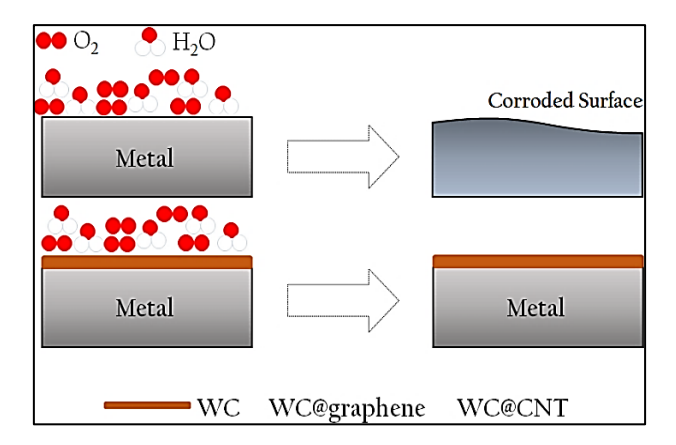


Figure 10. The ability of the synthesized samples in inhibition of corrosion

4. CONCLUSIONS

This study produced WC nanoparticles, and also the nanocomposites of WC@G and WC@CNT were synthesized in order to study their optical properties as well as corrosion inhibitory features. Different characterization tests were used to confirm their preparation.

The XRD pattern of WC nanostructures showed that they have a hexagonal phase (P-6m2) because of the crystal planes. When pure WC was mixed with graphene or CNTs, the main diffraction peak of those materials showed up. FESEM pictures showed that WC nanostructures had shapes that were not regular, and adding graphene or CNTs to them did not change their shapes. We also used Raman spectroscopy to make sure the samples were made right. Their Raman spectrum showed the main peaks that were linked to pure WC nanoparticles. On the other hand, the Raman spectra of WC@G and WC@CNT nanocomposites revealed each or both of D- and G-band, which were attributed to carbonaceous materials of graphene and CNTs.

Compositing pure WC improved its optical properties, which was ascribed to the role of graphene and CNTs in lowering the energy band gap of WC. Compositing also increased R_{ct} and shifted the open circuit potential to more

positive values, which causes corrosion. The tunable band structure of WC-based composites, together with their corrosion inhibition performance, suggests promising applications in environments where photoelectrochemical and barrier protection mechanisms may be synergistically exploited. Further studies are needed to decouple these effects.

REFERENCES

- [1] Wu, C.M., Naseem, S., Chou, M.H., Wang, J.H., Jian, Y.Q. (2019). Recent advances in tungsten-oxide-based materials and their applications. Frontiers in Materials, 6: 49. https://doi.org/10.3389/fmats.2019.00049
- [2] Kurlov, A.S., Gusev, A.I. (2013). Tungsten carbides. Springer Series in Materials Science, 184: 34-36. https://doi.org/10.1007/978-3-642-35464-0
- [3] Ahmad, N.A., Kamdi, Z., Tobi, A.L.M. (2018). Wear and corrosion behavior of tungsten carbide based coating on carbon steel. International Journal of Integrated Engineering, 10(4): 109-113. https://doi.org/10.30880/ijie.2018.10.04.018
- [4] Zhang, J., Saeed, M.H., Li, S. (2018). 13-Recent progress in development of high-performance tungsten carbide-based composites: Synthesis, characterization, and potential applications. Advances in Ceramic Matrix Composites, pp. 307-329. https://doi.org/10.1016/B978-0-08-102166-8.00013-X
- [5] Ahmad, S., Ashraf, I., Mansoor, M.A., Rizwan, S., Iqbal, M. (2021). An overview of recent advances in the synthesis and applications of the transition metal carbide nanomaterials. Nanomaterials, 11(3): 776. https://doi.org/10.3390/nano11030776
- [6] Bhosale, D.G., Rathod, W.S., Rukhande, S. (2018). Wear and oxidation behaviour of tungsten carbide based coatings: A review. In Proceedings of TRIBOINDIA-2018: An International Conference on Tribology, Faridabad Haryana, India.
- [7] Kamdi, Z., Voisey, K. (2016). Corrosion mechanism of tungsten carbide-based coatings in different aqueous media. Key Engineering Materials, 694: 167-171. https://doi.org/10.4028/www.scientific.net/KEM.694.16
- [8] Li, M., Song, Z., Gong, M., Mo, D., Wang, L., Dusza, J., Zhang, C. (2021). WC+ Co+ graphene platelet composites with improved mechanical, tribological and thermal properties. Ceramics International, 47(21): 30852-30859. https://doi.org/10.1016/j.ceramint.2021.07.266
- [9] Qi, W., Zhao, Z., Qian, Y., Zhang, S., et al. (2023). Effect of graphene on the microstructure and mechanical properties of WC-based cemented carbide. Crystals, 13(10): 1414. https://doi.org/10.3390/cryst13101414
- [10] Wei, Z., Wu, Y., Wei, Z., Wang, K., et al. (2022). The effect of bonding method between WC-Cr3C2-Ni and multiwall carbon nanotubes powders on the properties of composite coatings. Ceramics International, 48(20): 30996-31007. https://doi.org/10.1016/j.ceramint.2022.07.061
- [11] Li, W., Liu, W., Liu, Z., Wang, Z., et al. (2023). Effect of CNT content on the microstructure and friction characteristics of DED-fabricated CNTs-Ni60/WC coatings. Surface and Coatings Technology, 473: 129938. https://doi.org/10.1016/j.surfcoat.2023.129938

- [12] Liu, B., Sun, J., Zhao, J., Yun, X. (2025). Hybrid graphene and carbon nanotube–reinforced composites: polymer, metal, and ceramic matrices. Advanced Composites and Hybrid Materials, 8(1): 1. https://doi.org/10.1007/s42114-024-01074-3
- [13] Bakshi, S.R., Lahiri, D., Agarwal, A. (2010). Carbon nanotube reinforced metal matrix composites-A review. International Materials Reviews, 55(1): 41-64. https://doi.org/10.1179/095066009X12572530170543
- [14] Jung, H., Karmakar, A., Adhikari, A., Patel, R., Kundu, S. (2022). Graphene-based materials as electrocatalysts for the oxygen evolution reaction: A review. Sustainable Energy & Fuels, 6(3): 640-663. https://doi.org/10.1039/D1SE01716K
- [15] Liu, J., Sun, W., Huang, Y. (2021). Effect of carbon nanotubes content on microstructure and properties of WC/Ni laser cladding coatings. Surface Engineering, 37(5): 650-657. https://doi.org/10.1080/02670844.2020.1812481
- [16] Guan, H., He, X., Zhang, Z., Huang, J., Qu, X. (2024). Effect of tungsten carbide interface decoration on thermal and mechanical properties of carbon fiber reinforced copper matrix composites. Materials Today Communications, 41: 110810. https://doi.org/10.1016/j.mtcomm.2024.110810
- [17] Li, Y., Long, R., Tao, J., Chen, X., et al. (2025). Regulation of the interfacial structure in CNTs/Cu composites by chemical vapor deposited WC to enhance mechanical properties and conductivity. Ceramics International, 51, 23725-23740. https://doi.org/10.1016/j.ceramint.2025.03.060
- [18] Liu, T., Lyu, W., Li, Z., Wang, S., Wang, X., Jiang, J., Jiang, X. (2023). Recent progress on corrosion mechanisms of graphene-reinforced metal matrix composites. Nanotechnology Reviews, 12(1): 20220566. https://doi.org/10.1515/ntrev-2022-0566
- [19] Ovid'Ko, I.A. (2014). Metal-graphene nanocomposites with enhanced mechanical properties: A review. Reviews on Advanced Materials Science, 38(2): 86-101.
- [20] Say, Y., Guler, O., Dikici, B. (2020). Carbon nanotube (CNT) reinforced magnesium matrix composites: The effect of CNT ratio on their mechanical properties and corrosion resistance. Materials Science and Engineering: A, 798: 139636. https://doi.org/10.1016/j.msea.2020.139636
- [21] Hutapea, J.A.A., Manik, Y.G.O., Ndruru, S.T.C.L., Huang, J., Goei, R., Tok, A.I.Y., Siburian, R. (2025). Comprehensive review of graphene synthesis techniques: Advancements, challenges, and future directions. Micro, 5(3): 40. https://doi.org/10.3390/micro5030040
- [22] Pełech, I. (2010). Preparation of carbon nanotubes using CVD method. Polish Journal of Chemical Technology, 12(3): 45-49. https://doi.org/10.2478/v10026-010-0033-v
- [23] Aravinth, S., Sankar, B., Kamaraj, M., Chakravarthy, S. R., Sarathi, R. (2012). Synthesis and characterization of hexagonal nano tungsten carbide powder using multi walled carbon nanotubes. International Journal of Refractory Metals and Hard Materials, 33: 53-57. https://doi.org/10.1016/j.ijrmhm.2012.02.010
- [24] Kang, J.S., Kim, J., Lee, M.J., Son, Y.J., et al. (2017). Electrochemical synthesis of nanoporous tungsten carbide and its application as electrocatalysts for

- photoelectrochemical cells. Nanoscale, 9(17): 5413-5424. https://doi.org/10.1039/C7NR00216E
- [25] Cheong, Y.K., Calvo-Castro, J., Ciric, L., Edirisinghe, M., et al. (2017). Characterisation of the chemical composition and structural features of novel antimicrobial nanoparticles. Nanomaterials, 7(7): 152. https://doi.org/10.3390/nano7070152
- [26] Wang, X., Zhang, L. (2019). Green and facile production of high-quality graphene from graphite by the combination of hydroxyl radicals and electrical exfoliation in different electrolyte systems. RSC Advances, 9(7), 3693-3703. https://doi.org/10.1039/C8RA09752F
- [27] Siburian, R., Sihotang, H., Raja, S.L., Supeno, M., Simanjuntak, C. (2018). New route to synthesize of graphene nano sheets. Oriental Journal of Chemistry, 34(1): 182-186.
- [28] BinSabt, M., Shaban, M., Gamal, A. (2023). Nanocomposite electrode of titanium dioxide nanoribbons and multiwalled carbon nanotubes for energy storage. Materials, 16(2): 595. https://doi.org/10.3390/ma16020595
- [29] Ngoma, M.M., Mathaba, M., Moothi, K. (2021). Effect of carbon nanotubes loading and pressure on the performance of a polyethersulfone (PES)/carbon nanotubes (CNT) membrane. Scientific Reports, 11(1): 23805. https://doi.org/10.1038/s41598-021-03042-z
- [30] Alduwaib, S.M., Abd, M.M., Jalaukhan, A.H.A. (2022). The structural, optical, and self-cleaning properties of Mn₃O₄/SnO₂ multilayer thin films deposited using spray pyrolysis technique. Scientia Iranica, 28(6F): 3776-3785. https://doi.org/10.24200/sci.2021.56298.4650
- [31] Gabhale, B., Jadhawar, A., Bhorde, A., Nair, S., et al. (2018). High band gap nanocrystalline tungsten carbide (nc-WC) thin films grown by hot wire chemical vapor deposition (HW-CVD) method. Journal of Nano-and Electronic Physics, 10(3): 03018. https://doi.org/10.21272/jnep.10(3).03001
- [32] Hussain, S., Vikraman, D., Feroze, A., Song, W., et al. (2019). Synthesis of Mo₂C and W₂C nanoparticle electrocatalysts for the efficient hydrogen evolution reaction in alkali and acid electrolytes. Frontiers in Chemistry, 7: 716. https://doi.org/10.3389/fchem.2019.00716
- [33] Ikram, M., Raza, A., Imran, M., Ul-Hamid, A., Shahbaz, A., Ali, S. (2020). Hydrothermal synthesis of silver decorated reduced graphene oxide (rGO) nanoflakes with effective photocatalytic activity for wastewater treatment. Nanoscale Research Letters, 15(1): 95. https://doi.org/10.1186/s11671-020-03323-y
- [34] Das, P., Deoghare, A.B., Maity, S.R. (2021). A novel approach to synthesize reduced graphene oxide (RGO) at low thermal conditions. Arabian Journal for Science and Engineering, 46(6): 5467-5475. https://doi.org/10.1007/s13369-020-04956-y
- [35] Muniyalakshmi, M., Sethuraman, K., Silambarasan, D. (2020). Synthesis and characterization of graphene oxide nanosheets. Materials Today: Proceedings, 21: 408-410. https://doi.org/10.1016/j.matpr.2019.06.375
- [36] Jarvin, M., Kumar, S.A., Vinodhkumar, G., Manikandan, E., Inbanathan, S.S.R. (2021). Enhanced photocatalytic performance of Hausmannite Mn3O4-rGO nanocomposite in degrading methylene blue. Materials Letters, 305: 130750.

- https://doi.org/10.1016/j.matlet.2021.130750
- [37] Aziz, S.B., Marif, R.B., Brza, M.A., Hassan, A.N., et al. (2019). Structural, thermal, morphological and optical properties of PEO filled with biosynthesized Ag nanoparticles: New insights to band gap study. Results in Physics, 13: 102220. https://doi.org/10.1016/j.rinp.2019.102220
- [38] Messih, M.A., Ahmed, M.A., Soltan, A., Anis, S.S. (2019). Synthesis and characterization of novel Ag/ZnO nanoparticles for photocatalytic degradation of methylene blue under UV and solar irradiation. Journal of Physics and Chemistry of Solids, 135: 109086.
- https://doi.org/10.1016/j.jpcs.2019.109086
- [39] Zhai, Y., Guo, X., He, Y., Li, Z. (2023). Corrosion resistance and mechanical properties of electrodeposited Co-W/ZrO₂ composite coatings. International Journal of Electrochemical Science, 18(3): 100015. https://doi.org/10.1016/j.ijoes.2023.01.015
- [40] Umoren, P.S., Kavaz, D., Umoren, S.A. (2022). Corrosion inhibition evaluation of chitosan-CuO nanocomposite for carbon steel in 5% HCl solution and effect of KI addition. Sustainability, 14(13): 7981. https://doi.org/10.3390/su14137981